



A climatology of wave-breaking events with blocking flow configurations in the extratropical Southern Hemisphere

Ning Shi¹ · Tanimu Abubakar Sadiq^{2,3}

Received: 20 February 2024 / Accepted: 2 August 2024

© The Author(s), under exclusive licence to Springer-Verlag GmbH Germany, part of Springer Nature 2024

Abstract

Based on three daily reanalysis datasets for the period from 1958 to 2023, this study details the climatology of high-amplitude wave breaking (WB) events with blocking flow configurations over the extratropical Southern Hemisphere (SH). A given event is classified as a WB blocking high (WBBH) or blocking low (WBBL) event, depending on the polarity of the primary height anomaly center. Furthermore, these events are classified as an eastwards (E) type or westwards (W) type according to the longitudinal movement of the primary potential vorticity center. Both WBBH and WBBL occurrences are predominantly E-types. Specifically, E-type WBBH events are more frequent over the South Pacific and adjacent regions, such as the southeast Indian Ocean and southwest Atlantic. In contrast, E-type WBBL events tend to occur over the 45°S–60°S latitudinal band. On the other hand, W-type events are more likely to occur over the Antarctic continent. The distribution frequency of WB events is closely associated with the climatological mean flow, but no evident seasonal preference for their occurrence regions is observed. The composite results at several representative locations demonstrate a robust relationship between the anomalous potential vorticity flux at the primary potential vorticity center and the convergence/divergence of the wave-activity flux, reinforcing the understanding of the dynamics underlying these events.

Keywords Blocking · Rossby waves · Wave breaking · Synoptic climatology

1 Introduction

Wave breaking (WB) of Rossby waves is generally proposed from a morphology perspective, i.e., the irreversible deformation of material contours. Considering that material contours can deform in different configurations, WB is classified into anticyclonic or cyclonic orientations under the dominance of high- or low-pressure systems (Thorncroft et al. 1993; Peters and Waugh 1996; Tyrlis and Hoskins 2008; Masato et al. 2012). Since different types of WB may

correspond to different underlying dynamics and exert different influences, WB and its morphology have been the subject of many studies.

Pelly and Hoskins (2003) developed a WB index by calculating the macroscale meridional gradient of potential temperature around a reference latitude on the 2 PVU surface, which is regarded as the dynamical tropopause in the Northern Hemisphere (NH). Once the meridional gradient becomes poleward, the WB is considered to occur instantaneously and locally. The WB detected by the “PV- θ ” method is hereafter referred to as morphological WB. According to the folded orientation of PV or θ contours at the tropopause, early studies classified the morphological WB into anticyclonic and cyclonic types based on (1) the zonal gradient direction of θ (Masato et al. 2012), (2) the relative locations of the grid points along particular PV contours (Martius et al. 2007; Strong and Magnusdottir 2008; Rivière et al. 2010; Weijenborg et al. 2012), or (3) the direction of meridional wave-activity flux (Gabriel and Peters 2008; Ndarana and Waugh 2011).

Pelly and Hoskins (2003) were the first to propose that the morphological WB index can be used to detect blocking

✉ Ning Shi
shining@nuist.edu.cn

¹ Collaborative Innovation Center on Forecast and Evaluation of Meteorological Disasters, Key Laboratory of Meteorological Disaster of Ministry of Education, Nanjing University of Information Science & Technology, Nanjing, China

² School of Atmospheric Sciences, Nanjing University of Information Science and Technology, Nanjing, China

³ Nigerian Meteorological Agency (Nimet), Abuja, Nigeria

episodes if constraints on the spatial scale and temporal persistence are added to the morphological WB index. Although the robustness of the relationship between morphological WB and blocking has been questioned by several observational studies (Schwierz et al. 2004; Altenhoff et al. 2008; Small et al. 2014), the climatology of blocking and WB episodes, detected by the “PV- θ ” method, has been obtained for the NH (Tyrlis and Hoskins 2008; Gabriel and Peters 2008; Masato et al. 2013) and the SH (Berrisford et al. 2007; Ndarana and Waugh 2011).

Early studies have explored SH blockings or persistent anomalies from many perspectives. For example, blocking or persistent anomalies are prevalent over the South Pacific in austral winter (Trenberth and Mo 1985; Sinclair 1996; Renwick 2005; Berrisford et al. 2007; Liu et al. 2017); in austral summer, their maximum frequency appears over the West Pacific (Trenberth and Mo 1985; Renwick 2005; Berrisford et al. 2007). In terms of morphology, SH WB events can be divided into two broad types, i.e., anticyclonic and cyclonic, while there is no significant difference between different WBs in terms of equatorward or poleward PV intrusion (Ndarana and Waugh 2011). For external forcings, the El Niño–Southern Oscillation (Wiedenmann et al. 2002; Renwick 2005), Antarctic Sea Ice (Carpenedo and Ambrizzi 2022) and diabatic heating associated with deepening surface cyclones (Tilly et al. 2008) may play essential roles in modulating the variability or formation of SH blockings.

In contrast to the morphology perspective used in the abovementioned studies, some studies have proposed WB from a wave-activity perspective. Nakamura (1994) was the first to interpret the WB of Rossby wave trains as a dynamic process of wave activity, i.e., the accumulation and release of wave activity, as indicated by the convergence and divergence of wave-activity flux, respectively. This dynamic process of wave activity is evident in the evolution of the NH blocking highs but with some geographic and/or seasonal preferences (Nakamura et al. 1997; Nakamura and Fukumachi 2004; Takaya and Nakamura 2005; Wolf et al. 2018). In fact, the convergence/divergence of wave-activity fluxes is usually associated with anomalous potential vorticity (PV) fluxes (Holton 2004). Motivated by these results, we recently proposed a new detection scheme for WB events by using anomalous PV flux (Shi and Nakamura 2021; SN21 hereafter). Moreover, the composite analysis confirmed the consistency between the anomalous PV flux and the convergence/divergence of the wave-activity flux of quasi-stationary Rossby wave trains for the NH winter WB events.

Note that the WB or propagation of quasi-stationary Rossby wave trains has been documented in earlier studies on SH blocking. For example, the formation of austral spring and summer blockings (Renwick and Revell 1999) or a winter blocking event (Nishii and Nakamura 2004) over

the Southeast Pacific is associated with the WB of Rossby wave trains across the South Pacific. Apart from the Southeast Pacific, Hirasawa et al. (2000) reported that the amplification of blocking ridges over the interior of the eastern Antarctic continent in July 1997 was also associated with the WB of Rossby wave trains. However, we cannot conclude from these case studies that the WB of Rossby waves is generally important for the formation of blocking episodes over the SH. There is a lack of systematic analysis of SH WB events.

As a companion paper of SN21, this paper explores SH WB events from a wave-activity perspective. The remainder of this paper is organized as follows. After briefly describing our data and detection algorithms for WB events in Sect. 2, the results on the evolution of different types of SH WB events are given in Sect. 3. In Sect. 4, the influences of transient eddy feedback forcing and long-term variations in the occurrence frequency of WB events are discussed. The final section provides a summary.

2 Data and methods

2.1 Data

The long-term dataset used in this study was obtained from three reanalysis datasets, i.e., the Japanese 55-year Reanalysis (JRA55, Kobayashi et al. 2015), the fifth generation ECMWF reanalysis (ERA5, Hersbach et al. 2020) and the National Centers for Environmental Prediction/National Center for Atmospheric Research (NCEP/NCAR, Kalnay et al. 1996). All three reanalysis datasets are available globally on a regular longitude/latitude grid. The horizontal resolutions of the JRA55, ERA5 and NCEP/NCAR datasets used in the present study are 1.25°, 2.0° and 2.5°, respectively. Although both the ERA5 and NCEP/NCAR datasets provided longer time series, e.g., from 1940 to the present, only the common period among the three datasets from 1958 to 2023 was analysed. Overall, the results are similar among these three datasets. Therefore, only the results from the JRA55 are shown here. Parts of the results from the two other datasets are primarily provided in the Supplementary Material file.

The present study analysed the WB events for the austral spring (September–November, SON), summer (December–February, DJF), autumn (March–May, MAM) and winter (June–August, JJA). The following meteorological fields were used: (1) geopotential height, air temperature and wind velocity on isobaric surfaces and (2) PV and wind velocity on the 320 K isentropic surface. The 320 K isentropic surface is close to the upper troposphere/lower stratosphere

in the SH mid- and high latitudes throughout the year (not shown).

To focus on the low-frequency circulation associated with quasi-stationary Rossby wave trains, low-pass filtering is first applied to every meteorological field to remove high-frequency fluctuations associated with migratory transient disturbances with periods shorter than 8 days. Note that we also evaluated the feedback forcing of high-frequency disturbances on low-frequency fluctuations, which is discussed in Sect. 4.1.

Several studies have revealed a discontinuity around 1979 (Kidson 1999; Berrisford et al. 2007) and a long-term trend (Thompson and Solomon 2002; Renwick and Revell 1999) over the mid- and high-latitude SH in the reanalyses. Although observational data for the SH before 1979 are sparse, the reanalyses still provide us with the best estimates of the state of the global atmosphere and dynamically consistent syntheses of available global observations. In addition, there is a notable problem in the observational data over the SH from the late 1970s through the early 1990s (Seaman and Hart 2003), which may affect the accuracy of the reanalysis data. To minimize the potential influences of discontinuities, long-term variations or data quality problems, the climatological annual cycle for a given calendar date is calculated by a 31-day centred averaging of the 21-year daily climatology. The 21-yr running-mean climatology can make the latest period independent of the early period, which is important for circulation anomaly analysis. A local anomaly of a given variable on a particular date is then obtained by subtracting the climatological-mean annual cycle from its instantaneous low-frequency value. In the following text, the symbol prime indicates the low-frequency anomaly. The local standard deviation for a particular calendar date was obtained through a temporal sequence of 31

days/year \times 21 years = 651 days, where the annual 31-day sequence was centred on that particular day and the 21-year sequence centred on that particular year.

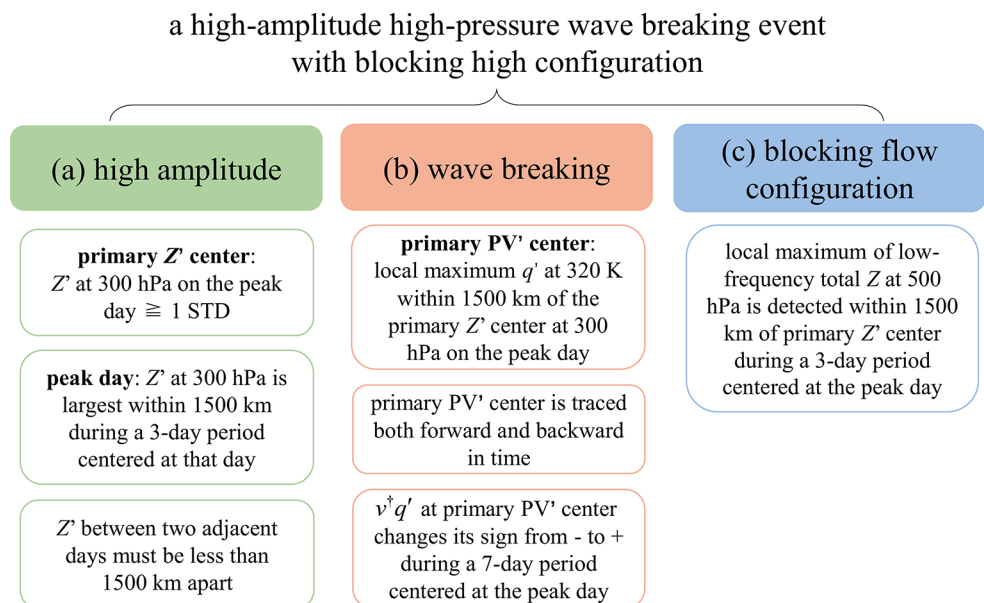
This study used the same shifting procedure as that employed in Nakamura et al. (1997) and SN21, which rotates a field along a great circle from a “target point” to the corresponding “reference point”. Such a shifting procedure can enhance the significance of composited local anomalies without causing any serious loss of geographical identity in the composited signatures. The definitions of both “target point” and “reference point” are given in Sect. 3.4. The significance of the composite analysis was assessed via the two-tailed t test. In the case of overoptimism in the significance tests over two-dimensional space, the false discovery rate (Wilks 2016) with the control level $\alpha_{FDR}=0.05$ is applied.

2.2 Detection scheme

As in SN21, the current study focuses on only those WB events that are characterized by (1) high amplitude, (2) WB from the wave-activity perspective and (3) blocking configurations. Both absolute and departure fields were used to identify high-amplitude WB events with blocking configurations, which was motivated by Barriopedro et al. (2010) and Dunn-Sigouin et al. (2013), who combined conventional total and departure approaches. A brief description of the detection scheme for WB events is provided here (Fig. 1).

A high amplitude is satisfied if the amplitude of the local height anomalies at 300 hPa (Z' for brevity) is larger than its local one standard deviation. Then, according to the positive or negative sign of Z' , the high-amplitude events poleward of 40°S are classified into two categories: high-pressure and low-pressure events. Note that these two types

Fig. 1 Schematic of the detection scheme for a high-amplitude wave breaking event with a blocking high configuration



are analogous to the “warm” and “cold” types of morphological WB, which are classified by Masato et al. (2012) according to the θ anomalies at the tropopause with respect to the climatological mean.

A high-pressure event is taken as an example to explicitly demonstrate the following identification algorithm. The peak day of a high-amplitude high-pressure event is identified if the local maximum of Z' is the largest over the region within 1500 km of the Z' center during a 3-day period centered at that peak day. The Z' center on the peak day is referred to as the primary Z' center. The primary Z' center was then traced backwards and forward in time to identify the start and end days. The start day is when the Z' value first exceeds e^{-1} (≈ 0.368) times the primary Z' value at the peak day, and the end day is when it falls below this threshold for the last time. Considering the quasi-stationarity of large-amplitude disturbances, the Z' centers between two adjacent days must be less than 1500 km apart, and the Z' centers on any given day should be within 2500 km of the primary Z' center on the peak day.

Theoretically, the divergence of the wave-activity flux $\nabla \cdot \mathbf{F}$ is associated with the PV flux $\mathbf{n} \cdot \mathbf{u}'q'$ (Takaya and Nakamura 2001), where \mathbf{n} denotes the local unit vector in the direction of the background PV gradient, $\mathbf{u}' = (u', v')$ is the small-amplitude wind anomaly superimposed on a steady zonally inhomogeneous background flow and q' is the PV anomaly. In the present study, $\mathbf{n} \cdot \mathbf{u}'$ is simplified as v^\dagger , which represents the component of the wind velocity anomaly perpendicular to the local climatological-mean flow. In other words, the local wind velocity anomaly $\mathbf{u}' = (u', v')$ in the longitude-latitude coordinate is transformed to v^\dagger in the new coordinate system, in which the X-axis and Y-axis are parallel and perpendicular to the climatological-mean flow, respectively. Accordingly, at the primary anomalous PV center for the blocking high, negative PV flux corresponds to the net convergence of wave-activity flux and the net accumulation of wave activity into a developing blocking ridge, zero PV flux indicates saturation around its peak day, and positive PV flux corresponds to downstream release of accumulated wave activity out of the decaying blocking ridge (Nakamura 1994; Nakamura et al. 1997; Nakamura and Fukamachi 2004). Based on the aforementioned knowledge, the WB feature is identified if the PV flux $v^\dagger q'$ at the primary anomalous PV center on the 320 K isentropic surface shifts its sign from negative to positive during the 7-day period centered at the peak day of a given high-amplitude event. For each high-amplitude high-pressure event, the center of the primary positive PV anomaly center on the 320 K isentropic surface is identified within the horizontal region within 1500 km of the positive Z' center on the peak day. The primary positive PV anomaly center is traced both forward and backward in time. The

distance between the primary PV anomaly centers on two adjacent days must be less than 1500 km.

The blocking flow configuration for a high-amplitude high-pressure WB event is considered to emerge if a local maximum in the low-pass-filtered total 500 hPa height field is detected within 1500 km of the primary Z' center in the 3-day period centered at the peak day (Nishii et al. 2011). In the following, a high-amplitude high-pressure WB event with a blocking flow configuration is referred to as a WBBH event. Analogously, a WBBL event refers to a high-amplitude low-pressure WB event with a blocking flow configuration in which a local minimum of the low-frequency 500 hPa height is detected.

Considering that different types of blocking exhibit distinct features in the zonal movement of the primary PV center (Tyrlis and Hoskins 2008; Masato et al. 2012), both the WBBH events and WBBL events are further classified according to the zonal movement of the primary PV anomaly center from day -3 to day 3 , i.e., $\Delta\lambda = \lambda_{day3} - \lambda_{day-3}$. λ is the longitude of the primary PV anomaly center. A WB event is regarded as the eastward (E) type if $\Delta\lambda \geq 10^\circ$. In contrast, it is regarded as the westward (W) type if $\Delta\lambda \leq -10^\circ$. The rest is referred to as the stationary type. We confirmed that the classification results are qualitatively unchanged if the other threshold values for $\Delta\lambda$ around 10° and other period lengths, such as 5 days (from day 2 to day -2) and 9 days (from day 4 to day -4), are set. Since the stationary type is rare for both the WBBH and WBBL events, the present study only focuses on the E and W types.

2.3 Wave-activity flux

The phase-independent wave-activity flux (Takaya and Nakamura 2001) was used to further verify whether high-amplitude WB events with blocking configurations are characterized by well-defined propagation of Rossby wave trains and whether the convergence/divergence of the wave-activity flux is consistent with the sign reversal of v^\dagger . For quasi-stationary perturbations, the flux on an isobaric surface may be expressed as follows:

$$F = \frac{p}{2|U|} \left(\begin{array}{l} U(\Psi_x'^2 - \Psi'\Psi'_{xx}) + V(\Psi_x'\Psi'_y - \Psi'\Psi'_{xy}) \\ U(\Psi_x'\Psi'_y - \Psi'\Psi'_{xy}) + V(\Psi_y'^2 - \Psi'\Psi'_{yy}) \\ \frac{f_0^2}{N^2}[U(\Psi_x'\Psi'_z - \Psi'\Psi'_{xz}) + V(\Psi_y'\Psi'_z - \Psi'\Psi'_{yz})] \end{array} \right)$$

where p = pressure/1000 (hPa), $\mathbf{U} = (U, V, \theta)$ is the climatological-mean seasonal cycle, f_0 is the Coriolis parameter at 45°N , ψ is the streamfunction, and N^2 is the squared buoyancy frequency. The subscripts represent partial derivatives. The primes indicate the low-frequency perturbations that are taken from the composited daily low-pass-filtered anomalies

associated with the high-amplitude WB events with blocking configurations. As noted by Wolf and Wirth (2017), the wave-activity flux is not strictly phase independent due to the semigeostrophic nature of Rossby wave trains. We thus focus on the net flux convergence/divergence around the primary PV anomaly center in the following analysis rather than on its local details.

3 Results

3.1 Frequency distribution

3.1.1 WBBH and WBL events

Figures 2 and 3 show the spatial distributions of the primary Z' centers on the peak day for the WBBH and WBL events, respectively, observed over the 66 years. At every

grid point, if the peak-day interval between two adjacent events is less than 8 days, the event with a smaller amplitude is discarded.

Clearly, WBBH events tend to occur mainly over the South Pacific and Antarctic throughout the year (first column of Fig. 2). In addition, they tend to occur over the southwest Atlantic Ocean in spring and winter and over the southeast Indian Ocean in summer and winter. Overall, this distribution is roughly consistent with earlier studies that identified the South Pacific as a preferential region for persistent anticyclonic anomalies (Trenberth and Mo 1985; Renwick 2005) or blocking high flows (Sinclair 1996; Berrisford et al. 2007; Liu et al. 2017). In addition, Fig. 2 also extends the case study of Hirasawa et al. (2000) from the climatological mean perspective that the Antarctic continent is another preferential region for WB events with blocking configurations. Note that the WBBH events occurring over the Antarctic continent differ from the traditional

Fig. 2 Frequency distributions of the center positions of various types of WBBH events from 1958 to 2023. A local value represents the total number of WB events identified within 500 km of a particular grid point. The first column shows the numbers of all WBBH events. The second column shows the number of E-type WBBH events, and the third column shows the number of W-type events. The rows represent austral spring (SON), summer (DJF), autumn (MAM) and winter (JJA). Thick blue (black) contours indicate that 90% (50%) of the total high-amplitude WB events exhibit blocking flow configurations, regarded as WBBH events. The hollow white circles in (e), (f) and (k) indicate the grid points where the composite analysis was applied in the following text. The domain is extended to 40S in all panels

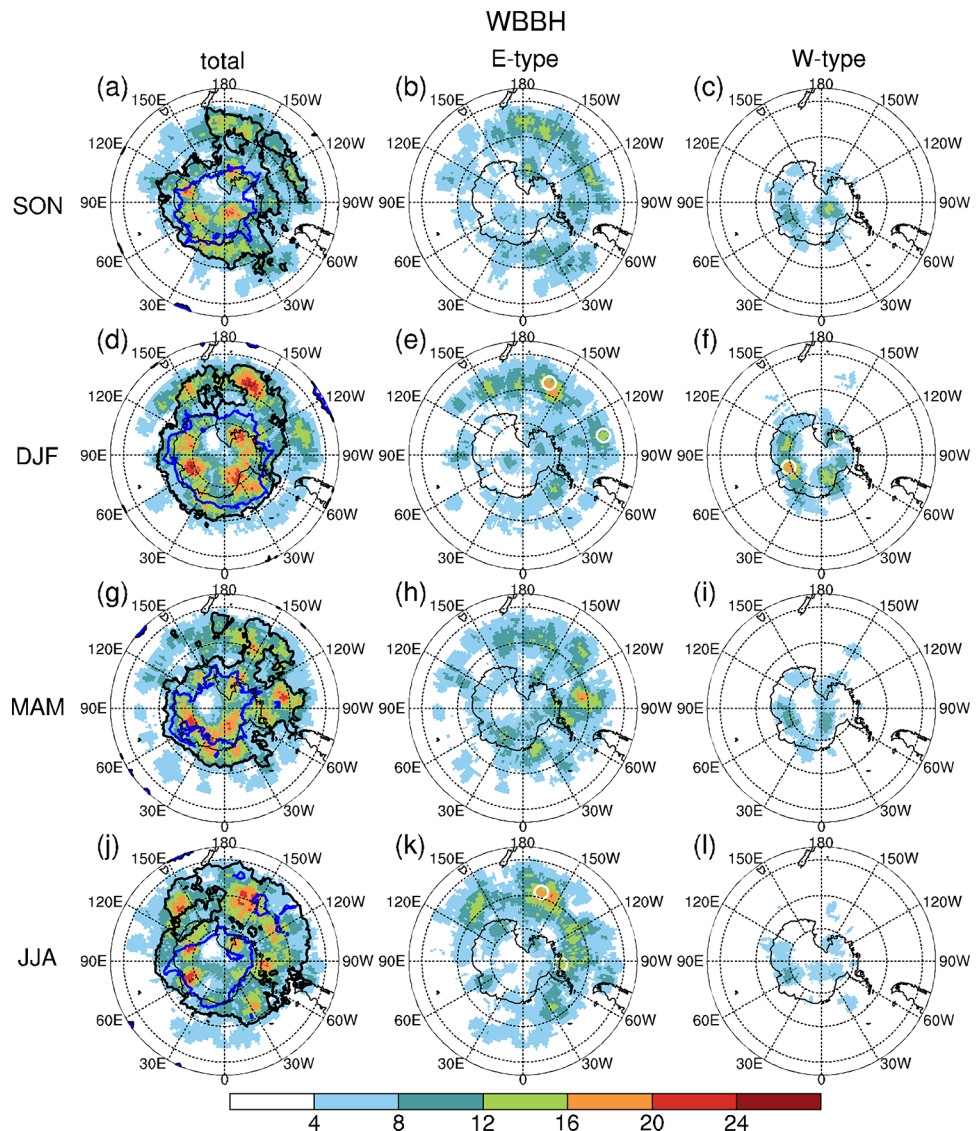
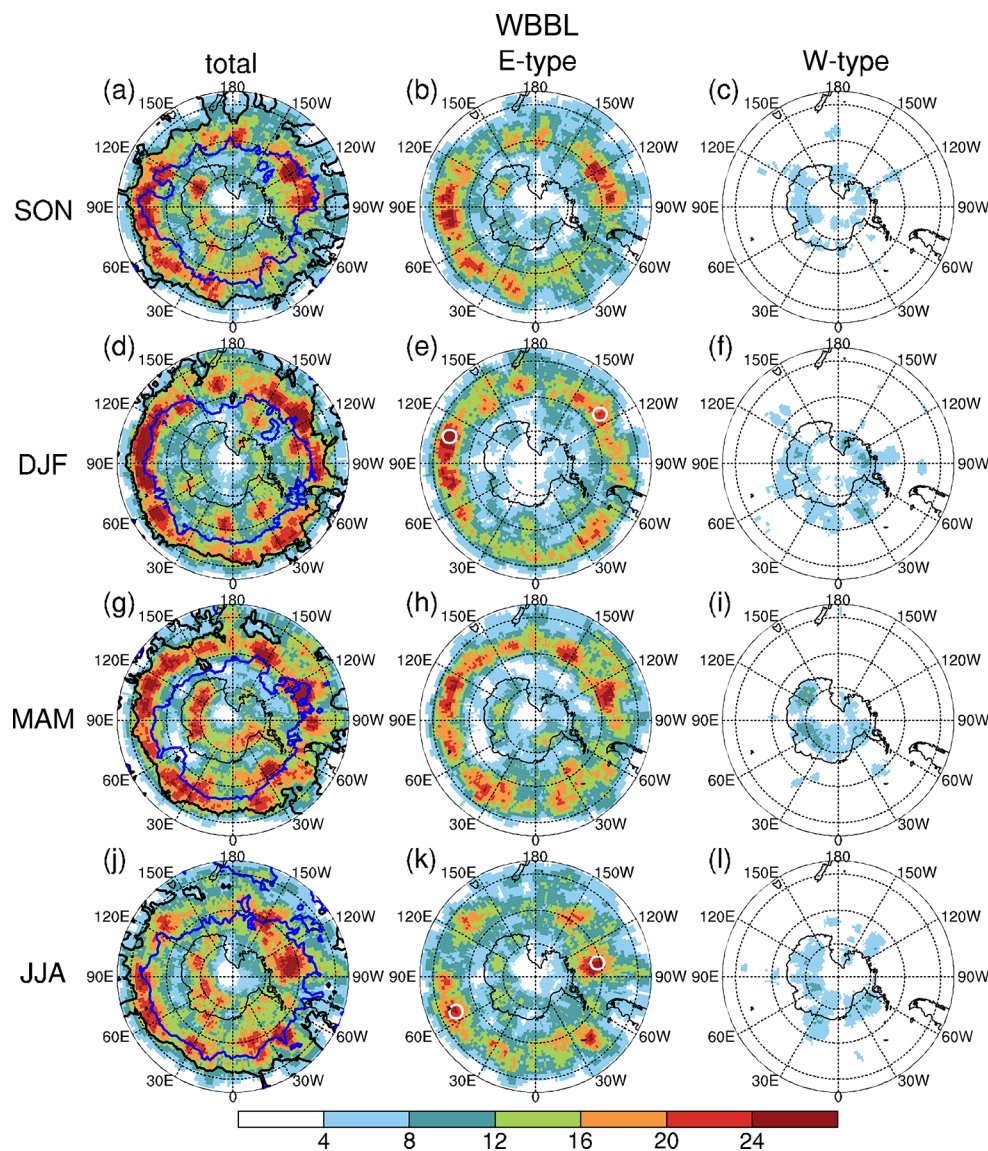


Fig. 3 As in Fig. 2 but for WBBL events



midlatitude blocking highs since they are located too far south to obstruct polar jet flow (first column of Fig. 4) or the passages of transient migratory eddies (third column of Fig. 4). Thus, these WBBH events can be regarded as high-latitude events (Berrisford et al. 2007).

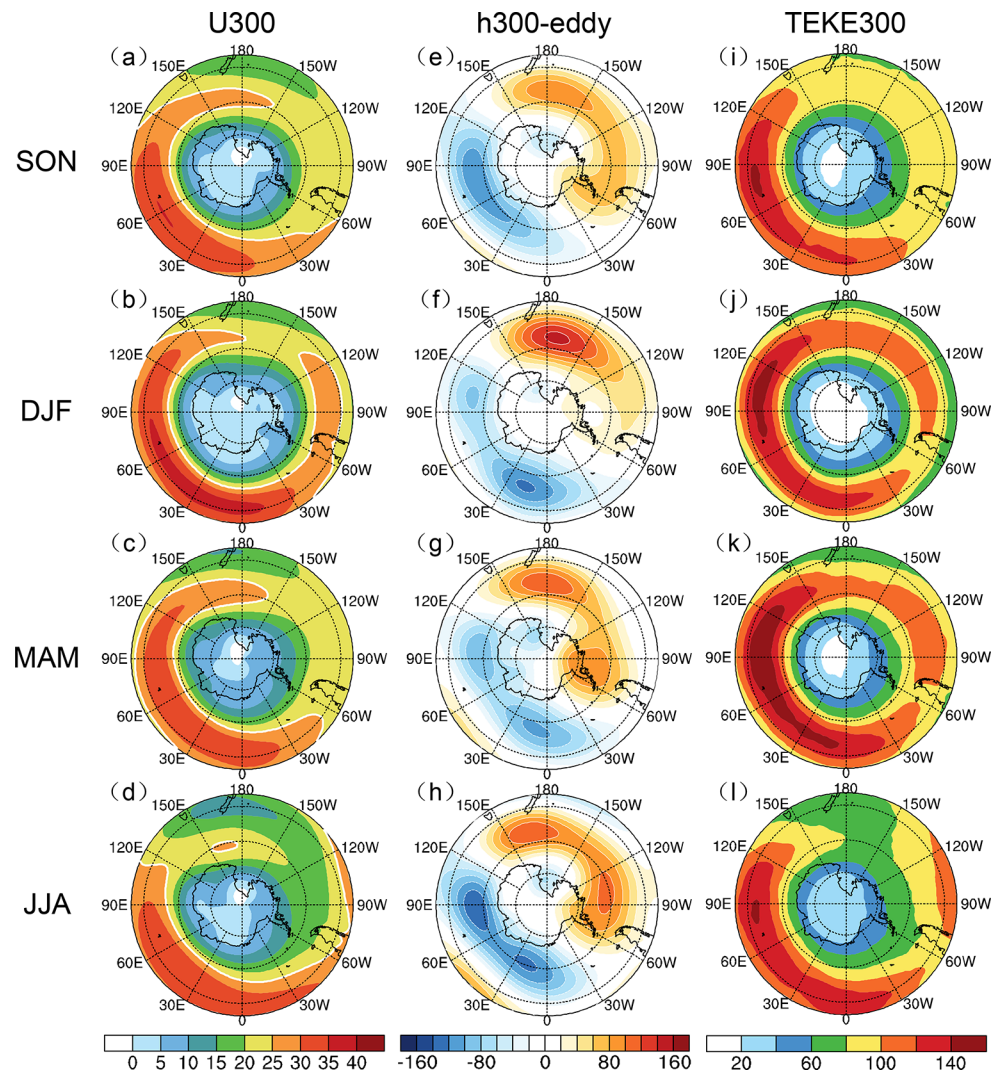
The WBBL events exhibited different distribution patterns. They are more uniformly distributed in midlatitude ocean regions and are predominantly concentrated within the latitudinal band of 45°S–60°S throughout the year (first column of Fig. 3). Interestingly, the Antarctic continent is also the preferential region for WBBL events, except in austral summer (Fig. 3d).

After further classifying the WB events into ‘E type’ and ‘W type’ based on the zonal movement of the primary PV anomaly center, it was observed that both the WBBH events and the WBBL events were predominantly characterized by the E type (second columns of Figs. 2 and 3). The E type

predominantly occurs in the mid- to high-latitude ocean, whereas the W type is more commonly found over the Antarctic continent (third columns of Figs. 2 and 3), which is particularly evident for WBBH events during summer (Fig. 2f).

Overall, the local peak frequency for both the WBBH and WBBL events is approximately 20 in the active regions. Consequently, both WBBH and WBBL events occur on average once every three years during each specific season over the most active regions. This frequency is less frequent than that of boreal winter WB events, which typically occur once every other winter season in the extratropical NH (SN21). Both the ERA5 and NCEP/NCAR datasets revealed similar frequency distributions for both the WBBH and WBBL events (Figs. S1–S4). The main difference was that the ERA5 data tended to identify more WB events, especially WBBH events, over the Arctic continent (Figs.

Fig. 4 (a–d) Climatological mean westerlies at 300 hPa, **(e–h)** departure of climatological mean geopotential height at 300 hPa from its zonal mean, and **(i–l)** climatological mean TEKE at 300 hPa for austral spring (SON, first row), summer (DJF, second row), autumn (MAM, third row) and winter (JJA, fourth row). Units are m/s for **(a–d)**, gpm for **(e–h)** and m^2/s^2 for **(m–p)**. The thick white lines in **(a–d)** indicate the contour at 25 m/s. The domain is extended to 40°S in all panels



S1 and S3), while the NCEP/NCAR data identified the lowest numbers of both WBBH and WBBL events (Figs. S2 and S4).

The occurrence frequency of WB events is much lower than that of blocking or WB events identified in previous studies. There might be three reasons for this discrepancy. First, the present study counted only the number of centers of the high-amplitude WB events. This is different from previous studies that considered the impact area of high-amplitude anomalies, WB events or persistent maxima (e.g., Trenberth and Mo 1985; Berrisford et al. 2007; Liu et al. 2017). Second, the number of events within 500 km of every grid point is counted. Thus, the spatial domain for identifying high-amplitude WB events at individual grid points is considerably more confined than the longitudinal sectors used by Wiedenmann et al. (2002), such as the Pacific sector spanning from 130°E to 60°W or the latitudinal band from 30°S to 70°S employed by Renwick (2005). Third, the constraint on the blocking flow configuration

reduced the number of WB events to a great extent (Figs. S5 and S6). In contrast, the constraint on the WB that requires a sign change in the anomalous PV flux only filtered out approximately 10–20% of the high-amplitude events with the blocking configurations. In other words, most of the blocking events over the SH are associated with Rossby wave propagation. Whether the WB events over the SH are more or less related to wave breaking processes than their NH counterparts still needs future quantitative comparison studies.

3.1.2 Reasons from background flow

If the blocking flow configurations (i.e., a local maximum of the low-pass-filtered total 500 hPa height field appears within 1500 km of the primary Z' center) are not considered, the number of high-amplitude high-pressure WB events is comparable to that of high-amplitude low-pressure WB events (Figs. S7 and S8). However, as shown in

Figs. 2 and 3, the number of WBBH events (with a blocking high configuration) is much lower than that of WBBL events (with a blocking low configuration), especially over the midlatitude South Atlantic and South Indian Oceans. To further discuss the circulation configurations of the WB events, the solid black and blue contours in the first columns of Figs. 2 and 3 denote the locations at which 50% and 90%, respectively, of the total high-amplitude WB events exhibit blocking flow configurations. The climatological mean flow southwards of 40°S in the four seasons is also shown in Fig. 4 to explore the reasons for the formation of the blocking flow configurations.

The percentage generally decreases equatorward for both high-pressure events and low-pressure events. Over the Antarctic continent, approximately 90% of both high-amplitude high-pressure WB events and high-amplitude low-pressure WB events are accompanied by blocking configurations (Figs. 2 and 3). Climatologically, the Antarctic continent is characterized by rather weak westerlies at 300 hPa (with speeds less than 10 m/s, first column of Fig. 4) and weak height eddies (heights deviating from their zonal mean at 300 hPa, second column of Fig. 4). This environment is equally favourable for a strong positive height anomaly to form a blocking high configuration (first column of Fig. 2) and for a strong negative height anomaly to form a blocking low configuration (first column of Fig. 3).

The climatological situation is different over mid- and high-latitude oceans. Both the polar jet and the height eddies exhibit evident geographical differences. During austral summer (Fig. 4b), the polar jet is at its strongest over the South Atlantic and Indian Oceans. Throughout the year (first column of Fig. 4), it spirals southwards toward Antarctica across the South Indian and Pacific Oceans, which might arise from momentum flux convergence associated with Rossby wave breaking (Williams et al. 2007). Positive eddies, corresponding to climatological high ridges, predominantly occur in the South Pacific, while negative eddies, which align with climatological low troughs, are primarily located in the South Atlantic and South Indian Oceans. Clearly, the combination of weak westerlies and a climatological high ridge over the South Pacific is favourable for strong positive height anomalies to form blocking high configurations. Approximately half of the high-amplitude high-pressure WB events in mid- to high-latitude oceans occur predominantly in the South Pacific (black contours in the first column of Fig. 2). Notably, during winter, the westerlies are at their weakest over the southeast Pacific (Fig. 4d), which explains the locally high percentage of blocking high configurations observed in that region (Fig. 2j).

Unlike the prevalence of blocking high configurations in the South Pacific, blocking low configurations tend to occur across nearly the entire mid- and high-latitude SH oceans,

as evidenced by the 50% contours at approximately 45°S (black contours in the first column of Fig. 3). It appears that westerlies and height eddies play competitive roles in the formation of blocking low configurations. Specifically, while the climatological low troughs over the South Indian Ocean and the South Atlantic are favourable for strong negative height anomalies to form blocking low configurations even though the local polar jet is strong, the weak westerlies similarly facilitate such a configuration over the South Pacific, even when there is a climatologically present high ridge. Consequently, blocking low configurations are more uniformly distributed across the extratropical SH than blocking high configurations are. Interestingly, both the 50% and 90% contours in Fig. 3 cover larger areas than those in Fig. 2. This indicates that blocking low configurations occur more frequently than blocking high configurations for high-amplitude WB events. This asymmetry in the formation of a blocking flow configuration is also observed in SN 21 and deserves further study.

Overall, the SH high-amplitude WB events defined from the wave-activity perspective are not necessarily accompanied by blocking flow configurations, which is similar to NH WB events (SN21). For simplicity, high-amplitude WB events with blocking flow configurations are referred to as WB events in the following analysis.

3.1.3 Dependence on the amplitude

As shown in Fig. 2, the occurrence frequency of extratropical WBBH events in summer is comparable to that in winter, which might contradict previous findings that blocking highs are more frequent in austral winter (Trenberth and Mo 1985; Wiedenmann et al. 2002; Renwick 2005; Berrisford et al. 2007). To investigate this discrepancy, Fig. 5a shows the frequency distributions of the WBBH events according to their amplitude. Evidently, moderate amplitudes within the range of 300 to 400 gpm constitute the largest proportion across all seasons, with comparable numbers of WBBH events throughout the four seasons. However, when considering weak-amplitude bins (e.g., 100–200 and 200–300 gpm), austral summer emerges as the most active season, while austral winter is the least active season. Note that these weak amplitudes predominantly occur at high latitudes where the local standard deviation is relatively small (not shown). On the other hand, for large-amplitude ranges such as 400–500 gpm, austral winter becomes the most active season, while spring and summer become the least active. Thus, the greater number of WBBH events observed in austral summer than in winter is mainly due to the inclusion of weak-amplitude events occurring primarily over high latitudes. Indeed, if a larger threshold value, e.g., 400 gpm, is used instead of the local one standard deviation as

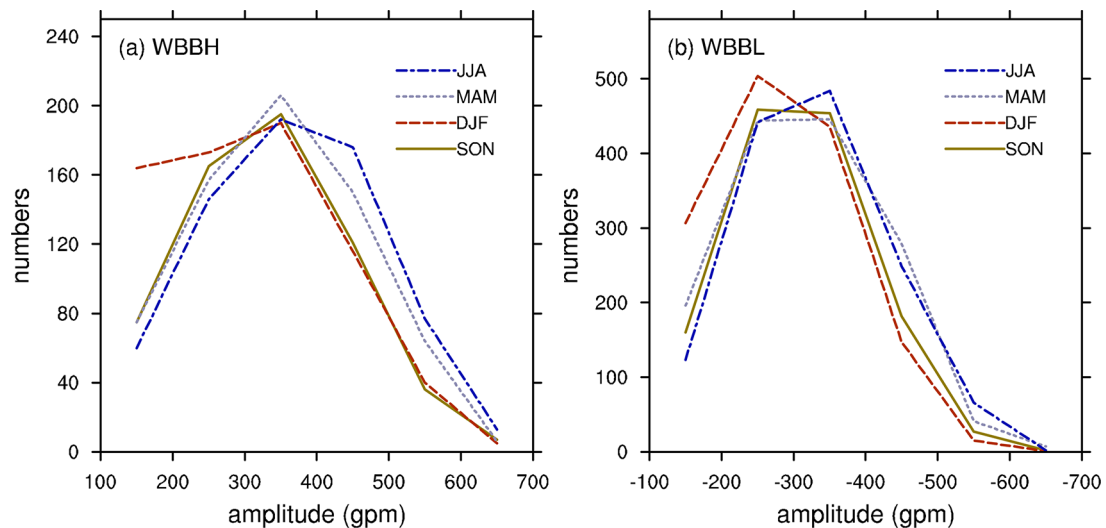


Fig. 5 Frequency distributions of (a) WBBH events and (b) WBBL events with their primary h300 anomalies within a given amplitude range

the minimum amplitude for defining WBBH events, similar seasonal frequency distributions to those reported in earlier studies would be obtained (not shown). The WBBL events exhibited a similar frequency distribution (Fig. 5b). Austral summer remains the most active season for weak-amplitude bins, while austral autumn and winter are the active seasons for large-amplitude bins. In fact, both the ERA5 data and NCEP/NCAR data revealed similar results (Figs. S5 and S9). However, both of these datasets revealed that the number of moderate-amplitude WBBH events, with intensities ranging from 300 to 400 gpm, peaked in winter, rather than in autumn as revealed by the JRA55 (Fig. 5a).

3.2 Characteristic time scale

To objectively determine the characteristic time scale of the SH WB events, a semi-log plot was generated. Early studies (Dole and Gordon 1983; Pelly and Hoskins 2003; Barriopedro et al. 2010) have shown that blocking events can be considered as a first-order Markov process, where the probability of an event lasting n days and continuing to $n + 1$ day is independent of n . The reciprocal of the linear slope of the logarithmic profile of the cumulative blocking histogram can be regarded as the characteristic time scale of blockings. Accordingly, Fig. 6 shows the semi-log plots of the cumulative histogram (i.e., the number of WB episodes lasting equal to or longer than a given duration bin). An evident exponential distribution of blocking persistence is observed within the duration range from 9 to 25 days. The reciprocal of the linear slope in these semi-log plots is approximately 5–6 days, which is considered the characteristic time scale for SH WB events. This time scale is significantly shorter than the 9 days for boreal winter NH WB events (SN21), which is consistent with the more transient nature of SH

blocking events (Berrisford et al. 2007). The longest characteristic time scales occur in austral summer, amounting to 6.6 days for the WBBH events and 5.8 days for the WBBL events. The ERA5 data and NCEP/NCAR data revealed similar characteristic time scales (Table S1 of the Supplementary Material). The evident differences among the three reanalysis datasets occurred in the austral summer. The time scales of both the WBBH and WBBL events depicted by ERA5 are approximately one day longer than those by the two other reanalysis datasets.

3.3 Composite analysis

In this section, composite analysis was applied for different types of WB events to determine whether they tend to accompany incipient Rossby waves. Due to the similarities among the four seasons, only the composite results during the austral summer and winter at several representative locations are presented. Additionally, motivated by the findings of SN21 on NH WB events, the evolution of the total fields for these WB events is discussed to examine their correspondence with the anticyclonic or cyclonic WB features as proposed from a morphological perspective (e.g., Thorncroft et al. 1993; Peters and Waugh 1996; Peters and Waugh 2003; Tyrlis and Hoskins 2008; Masato et al. 2013).

To enhance the significance of the composite results, the shifting procedure (Nakamura et al. 1997) was implemented prior to the composite process. Specifically, circulation fields are shifted along the great circle from a unique “target point” to a predefined “reference point” for each WB event. The reference points chosen are representative locations, depicted by hollow white dots in Figs. 2 and 3. For every WB event within a 500 km radius of its corresponding reference point, the target point is the grid point where

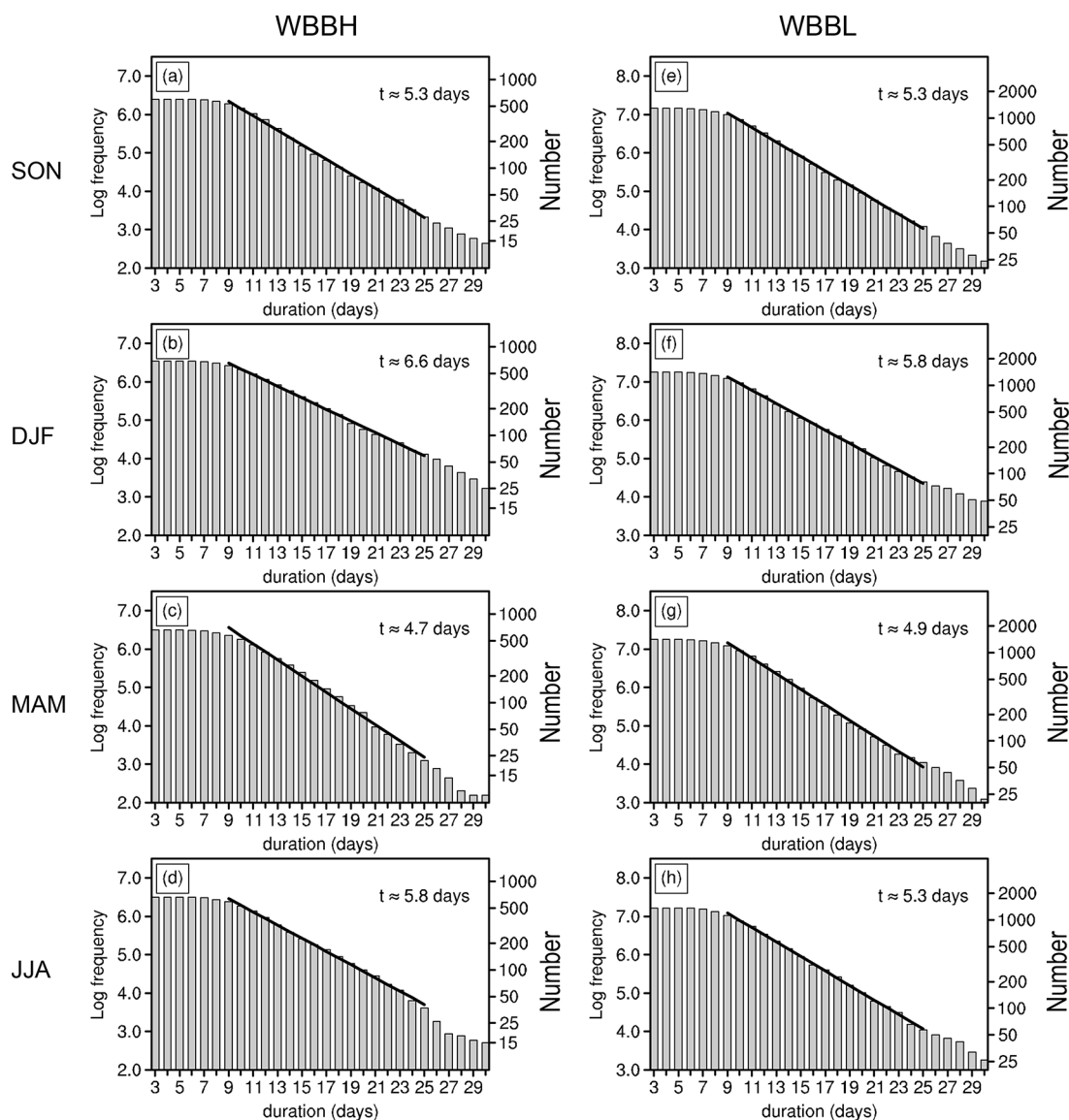


Fig. 6 Log (to base e) plot of the cumulative numbers of (a–d) WBBH events and (e–h) WBBL events lasting a given number of days. The results from the first row to the fourth row are for austral spring (SON), summer (DJF), autumn (MAM) and winter (JJA). The right ordinate in

each panel indicates the cumulative numbers. The thick solid lines in each panel indicate linear regressions for high-amplitude WB events with durations ranging from 9 to 25 days

the primary Z' center is located on the peak day. The spatial shifting is also applied to all temporal lags in the same manner.

For convenience, $-N$ (N) days represent the N days before (after) the peak day for a given WB event. Note that the composite circulation anomalies generally lack statistical significance before day -4 and after day 4. Hence, the following composite evolutions of the WB events are shown from day -4 to day 4 with an interval of 2 days.

3.3.1 E-type WBBH events in summer

The maximum frequency of E-type WBBH events in summer is 19, which is observed in the southwest Pacific at $[55^{\circ}\text{S}, 200^{\circ}\text{E}]$, as shown in Fig. 2e. The first two columns of Fig. 7 show the composited evolution of these 19 E-type WBBH events. In the developing stage, the primary positive PV anomaly stays under the northerlies (<0 , hatched in Fig. 7f, g), which is on the upstream flank of the amplifying pressure ridge over the southwest Pacific (Fig. 7a, b). This results in an anomalous negative PV flux (<0). Consistently, the wave-activity flux from upstream converges over the southwest Pacific (blue shading in Fig. 7a, b). At the

peak time (day 0, Fig. 7h), the anomalous PV flux weakens as the PV anomaly center is located almost where $= 0$. Correspondingly, there is either no net or very weak net flux divergence near the primary PV anomaly center, as it is enveloped by wave-activity flux convergence and divergence of similar intensities (Fig. 7c). In the decay stage, the primary PV anomaly center shifts eastwards into a region of anomalous southerlies, thereby generating a positive anomalous PV flux (> 0 ; Fig. 7i, j). Concurrently, the wave activity flux diverges from the vicinity of the decaying PV anomaly (Fig. 7d, e).

Renwick and Revell (1999) demonstrated that the propagation of Rossby wave trains across the South Pacific is pivotal to the formation of austral summer blocking over the southeast Pacific. To substantiate these findings, the last two columns of Fig. 7 depict the composited evolution of 14 E-type WBBH events identified at $[52.5^{\circ}\text{S}, 256.25^{\circ}\text{E}]$.

The consistency between the anomalous PV flux and the propagation of a Rossby wave train around the primary PV anomaly center becomes even more evident. Specifically, as at the primary positive PV anomaly center changes from negative in the developing stage (Fig. 7p, q) to positive in the decay stage (Fig. 7s, t), the wave-activity flux surrounding the primary PV anomaly center gradually transitions from convergent (Fig. 7k, l) to divergent (Fig. 7n, o).

Note that for the E-type WBBH events over the southeast Pacific (last two columns of Fig. 7), the high ridge extends southeastward and exhibits a pronounced macroscale overturning feature in the total height field (Fig. 7m, n). From a morphological perspective (Berrisford et al. 2007), this overturning feature should be classified as an anticyclonic WB. In line with Ndarana and Waugh (2011), this anticyclonic WB characteristic is also suggested by the northwards direction of the meridional wave-activity flux across

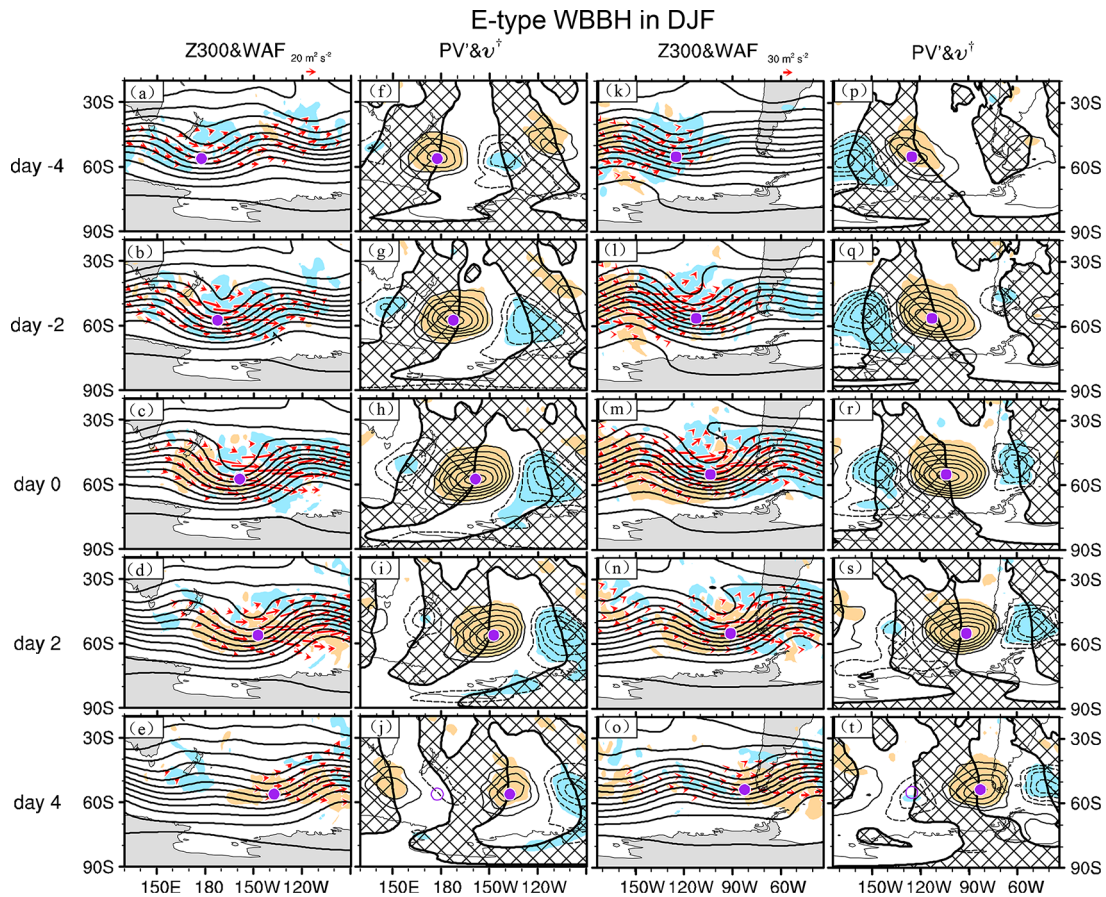


Fig. 7 Composite evolutions of the E-type WBBH events in the austral summer season (DJF). The first two columns are for 19 events at $[55^{\circ}\text{S}, 200^{\circ}\text{E}]$, and the last two columns are for 14 events at $[52.5^{\circ}\text{S}, 256.25^{\circ}\text{E}]$. The first and third columns are the geopotential height and wave-activity flux (WAF) at 300 hPa, respectively, and the second and fourth columns are the PV anomaly and anomalous wind velocity (v^{\dagger}) on the 320 K surface. The filled purple dots indicate the primary low-PV anomaly centers at a given lag, while the purple open circles in (h), (j), (r) and (t) denote the corresponding centers on day -4 . The

blue and orange shading represent the convergence and divergence, respectively, of the WAF (first and third columns). In the second and fourth columns, the blue and orange shading represent positive and negative PV anomalies, respectively, which are significant at the 5% level. Hatching in the second and fourth columns indicates the equatorward anomalous wind ($v^{\dagger} < 0$). The contour intervals are 100 m in the first and third columns and $4 \times 10^{-7} \text{ K m}^2 \text{ kg}^{-1} \text{ s}^{-1}$ in the second and fourth columns. For a WAF with an amplitude less than $10 \text{ m}^2 \text{ s}^{-2}$, the contours of zero PV anomalies are omitted

the overturning area. However, for the E-type WBBH events over the southwest Pacific, the high ridge primarily advances poleward without a clear overturning feature (Fig. 7b-d). Consequently, it should be noted that E-type WBBH events, as defined by our detection method, are not always synonymous with the anticyclonic type of morphological WB.

3.3.2 W-type WBBH events in summer

As shown in Fig. 2f, there are four locations across the Antarctic continent where the local frequency of W-type WBBH events in summer exceeds 12. The highest frequency, amounting to 19 events, is detected over the eastern Antarctic continent at [73.75°S, 70°E]. The first two columns of Fig. 8 show the composited evolution of these 19 W-type WBBH events. The last two columns of Fig. 8 present the composite results for another set of 12 W-type WBBH events that occurred over the western Antarctic continent at [77.5°S, 223.75°E].

From day -4 to day 0 (Fig. 8a-c), a pressure ridge develops and extends southwestward over the eastern Antarctic continent, which is associated with the convergence of

the wave-activity flux pointing southeastward. An isolated anticyclonic vortex emerges and sustains over the eastern Antarctic continent from approximately day -2 to day 4 (Fig. 8b-e). After the peak day, the wave-activity flux starts to diverge more prominently, corresponding to the weakening of the blocking high. Note that the anomalous PV flux v^{\dagger} at the primary PV anomaly center transitions from negative on day -4 (Fig. 8f) to positive on day 4 (Fig. 8j), dynamically aligning with the net convergence of the wave-activity flux observed before day -2 (Fig. 8a) and subsequent divergence occurring after day 2 (Fig. 8e) in the vicinity of the primary PV anomaly center.

In contrast to those over the eastern Antarctic continent, WB events occurring over the western Antarctic continent exhibit substantial upstream wave-like anomalies embedded within the polar jet before day 0 (Fig. 8p, q). The wave-activity flux diverges from the upstream pressure ridge situated southeast of New Zealand and converges into the southeast Pacific before the peak day (Fig. 8k, l). As a result, the pressure ridge over the southeast Pacific strengthens and extends southwestward. After the formation of the isolated anticyclonic vortex on day 0 (Fig. 8m), the divergence of the wave-activity flux gradually overtakes the convergence

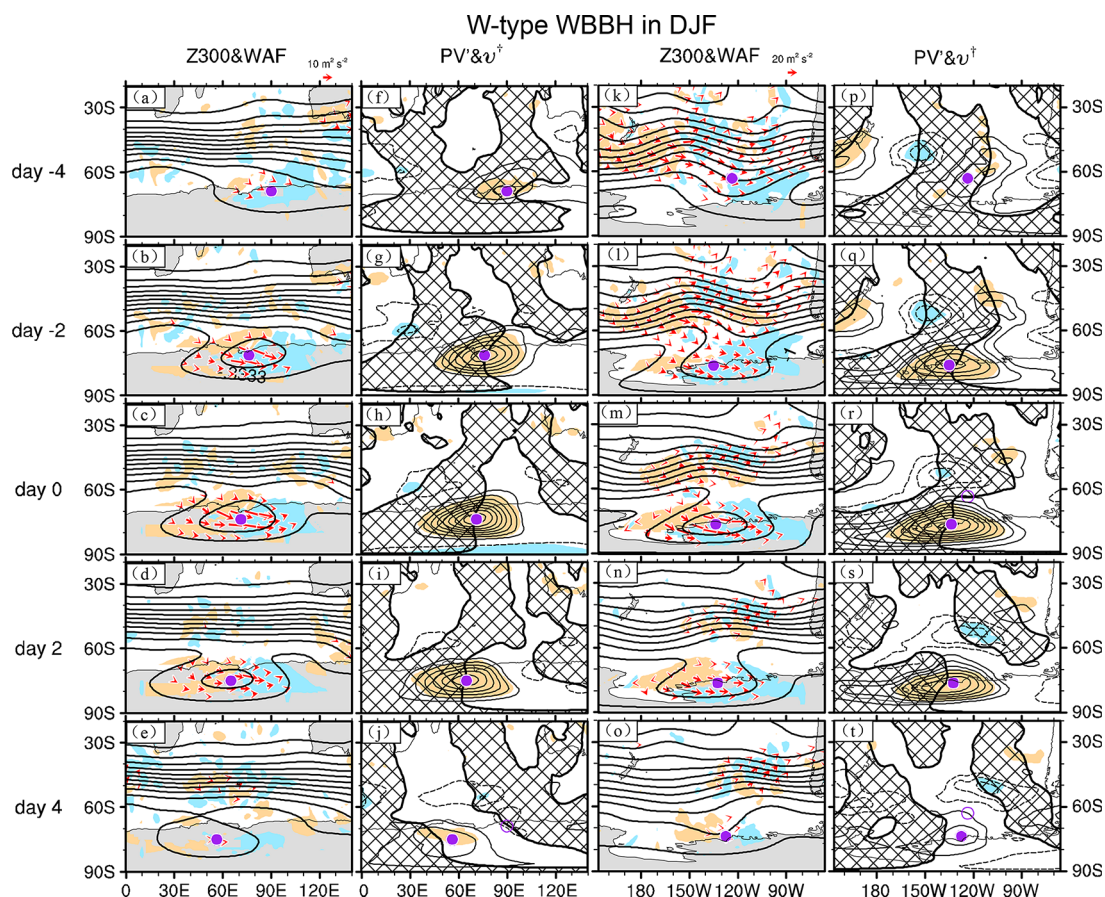


Fig. 8 As in Fig. 7, but for 19 W-type WBBH events at [73.75°S, 70°E] (first and second columns) and 12 W-type WBBH events at [77.5°S, 223.75°E] in austral summer, and WAF events with amplitudes less than $3 \text{ m}^2 \text{ s}^{-2}$ are omitted in (f-g)

(Fig. 8n, o). As in the eastern Antarctic case, at the primary PV anomaly center, the anomalous PV flux also underwent a sign change from negative (Fig. 8p, q) to positive (Fig. 8s, t). Hence, the dynamic consistency between the anomalous PV flux and the wave-activity flux also remains valid for these western Antarctic WB events.

Note that for W-type WBBH events over both the eastern and western Antarctic continents, the primary PV anomaly centers typically exhibit a southwestward movement, which coincides with the development of a distinct cyclonic overturning pattern. In fact, the cyclonic overturning feature is accompanied by a poleward-directed meridional wave-activity flux, aligning with the findings of early studies (Gabriel and Peters 2008; Ndarana and Waugh 2011).

3.3.3 E-type WBBH events in winter

For winter E-type WBBH events, a composite analysis was carried out separately at two representative locations, i.e., [57.5°S, 195°E] (first two columns of Figs. 9) and [72.5°S, 275°E] (last two columns of Fig. 9). The former site, located in the southwest Pacific, experiences the highest frequency, with 19 occurrences, while the latter, situated at a higher

latitude near the Antarctic Peninsula, records a local maximum frequency of 16. Notably, the latter location [72.5°S, 275°E] is also in close proximity to the region identified by Renwick (2005) as having the maximum frequency of persistent height anomalies during the austral winter season.

The evolution of the WBBH events at both representative locations is characterized by the propagation of Rossby wave trains. Before the peak day, the wave-activity flux from upstream along the polar jet converges near the primary PV anomaly center (Fig. 9a, b, k, l), leading to amplification of the pressure ridge. Similarly, the WBBH events around the Antarctic Peninsula also feature southeastward propagation of Rossby wave trains (Fig. 9k, l). Consequently, the high ridge extends further poleward around the Antarctic Peninsula (Fig. 9k-m). During the decay stage, for the WBBH events in the southwest Pacific, Rossby wave trains spread both southeastward and northeastward (Fig. 9c-e), contributing to the deepening of the downstream pressure trough (Fig. 9c-e) and the formation of negative PV anomalies with a distinctive “right bracket” shape to the northwest of the Antarctic Peninsula (Fig. 9h-j). In contrast, for the WBBH events around Antarctic Peninsula, Rossby wave trains tend to be reflected northeastward (Fig. 9n) after reaching their

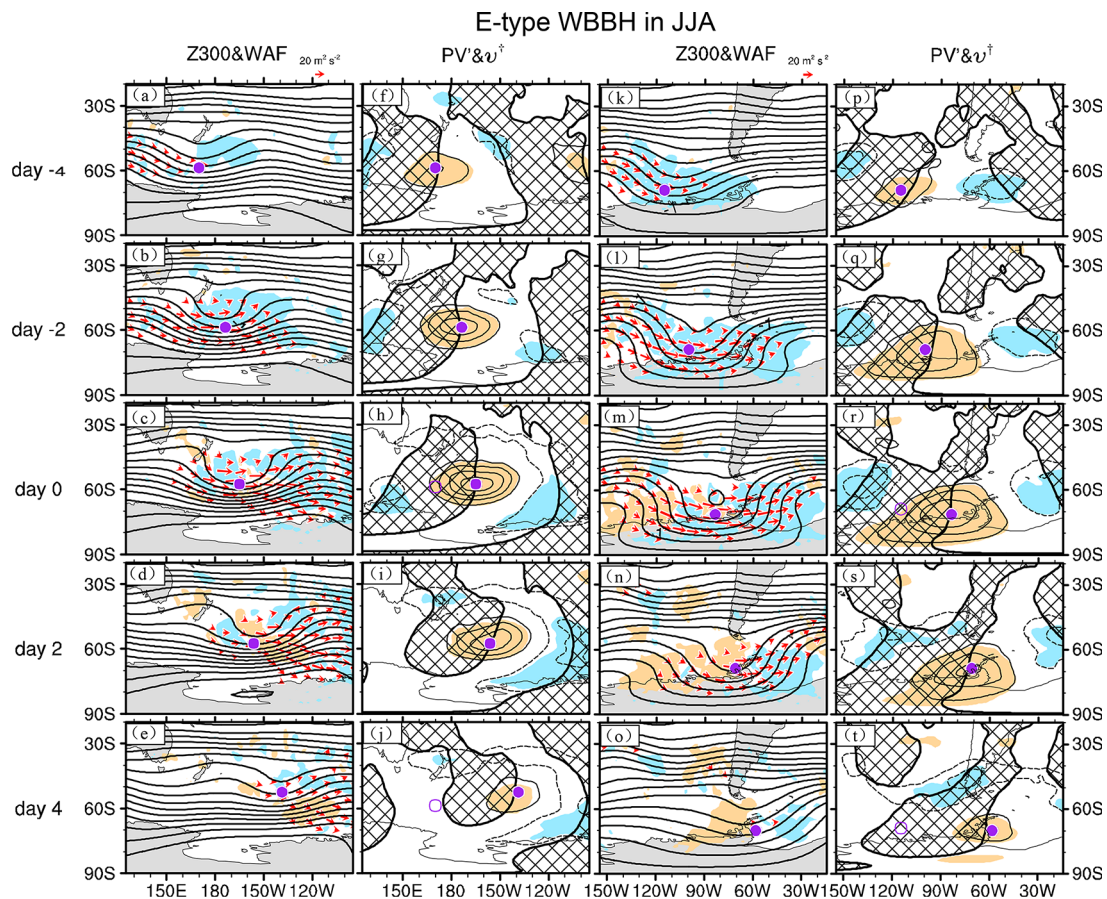


Fig. 9 As in Fig. 7, but for 19 E-type WBBH events at [57.5°S, 195°E] (first and second columns) and 16 E-type WBBH events at [72.5°S, 275°E] in the austral winter (JJA)

southernmost latitude at approximately day 0 (Fig. 9m). This reflection supports the occurrence of negative PV anomalies downstream (Fig. 9s).

Although there are differences in the propagation features of Rossby wave trains, the consistency between the sign of the anomalous PV flux and the convergence/divergence of the wave-activity flux remains robust for WBBH events at both locations. In line with the converging wave activity flux, the anomalous PV flux v^\dagger at the primary PV anomaly center is negative because the positive PV anomaly center resides in the northerly region (Fig. 9f, p and q). After day 0, as the primary positive PV anomaly center migrates into southerly regions ($v^\dagger < 0$), the anomalous PV flux v^\dagger becomes positive (Fig. 9j, s, t), which corresponds to the net divergence of the wave-activity flux around the primary PV anomaly center (Fig. 9d, e, n, o). This mutual correspondence highlights the underlying dynamics governing the evolution of WBBH events across different latitudes and geographic locations.

In the total height field, WBBH events occurring over the southwest Pacific predominantly display a poleward-extending amplifying ridge without any conspicuous overturning features or clear anticyclonic/cyclonic WB characteristics (first column of Fig. 9). This pattern is similar to that of the E-type WBBH events in austral summer in the southwest Pacific (first column of Fig. 7). This similarity between the two seasons may be attributed to the local mixture of anticyclonic and cyclonic WB features, as noted by Berrisford et al. (2007). However, for the WBBH events around the Antarctic Peninsula, the amplifying pressure ridge exhibits an omega shape with an anticyclonic overturning feature on its upstream flank and a cyclonic overturning feature on its downstream flank (Fig. 9m). Thus, it is challenging to definitively categorize these events into either anticyclonic or cyclonic WB types from a morphological perspective.

3.3.4 E-type WBBL events in summer

The location with the highest frequency of E-type WBBL events in summer is [50°S, 107.50°E], where 30 events are observed. This location is situated in the exit region of the polar jet (Fig. 4b). The first two columns of Fig. 10 present the composite evolution of these 30 events. For comparative purposes, a similar composite analysis was conducted for another set of 24 E-type WBBL events at [53.75°S, 232.5°E] over the South Indian Ocean (last two columns of Fig. 10), which is the entrance region of the polar jet (Fig. 4b).

In terms of both the evolution of the PV anomalies and Rossby wave propagation, the two categories of E-type WBBL events closely resemble each other. These fluctuations are manifested mainly as an enhanced and north-eastward-extending polar vortex, which is associated with

the propagation of Rossby wave trains along the polar jet. Accordingly, the negative PV flux at the primary PV center (Fig. 10f, p) is consistent with the net convergence of the wave-activity flux near the primary negative PV anomaly center before the peak day (Fig. 10a, b, k, l). After the peak day (Fig. 10d, c, n, o), the anomalous positive PV flux (Fig. 10i, j, s) aligns with the net divergence of the wave-activity flux.

However, there is a difference between the two regions. Over the southeast Indian Ocean, Rossby wave trains begin propagating northeastward around day -2 (Fig. 10b, c). Due to the convergence of the wave activity flux, the downstream high ridge amplifies and extends southwestward. Together with the northeastward extension of the upstream pressure trough, a cyclonic breaking feature emerges on day 0 (Fig. 10c). In contrast, for WBBL events over the southeast Pacific, the pressure trough amplified equatorward without a clear overturning feature.

3.3.5 E-type WBBL events in winter

Two representative locations are selected for the composite analysis of the E-type WBBL events in winter, i.e., [51.25°S, 66.25°E] and [61.25°S, 257.5°E]. The events occur most frequently at the former location (28 times) and the latter location (27 times) (Fig. 3k). As shown in Fig. 4b, the former location is at the polar jet core, while the latter is poleward of the subtropical jet.

Overall, the composite evolutions for the two categories of E-type WBBL events also closely resemble each other (Fig. 11). For example, the polar vortex tends to enhance and extend northeastward, which is associated with the convergence of the wave-activity flux; the contours of the height field begin to overturn cyclonically at approximately day -2 (Fig. 11b, l). More importantly, the consistency between the sign change in the anomalous PV flux and the convergence/divergence of the wave activity flux is also confirmed during evolution for both categories. Note that the Rossby wave trains tend to propagate northeastward in the vicinity of the primary negative PV center after day 0 (Fig. 11c, d, m-o), which might be associated with the stronger climatological westerlies (Fig. 4d) northeastward of the primary negative PV center than they are AROUND THE PRIMARY NEGATIVE PV CENTER.

Distinct differences in their evolutions are also observed. For the WBBL events over the southern Indian Ocean, upstream circulation anomalies are embedded within the polar jet (Fig. 11g, h), causing Rossby wave trains to primarily propagate zonally along the strong polar jet before day 0 (Fig. 11b, c). In contrast, over the central Pacific, the amplifying pressure ridge at approximately 140°W diverts the subtropical jet poleward, facilitating a southeastward-directed

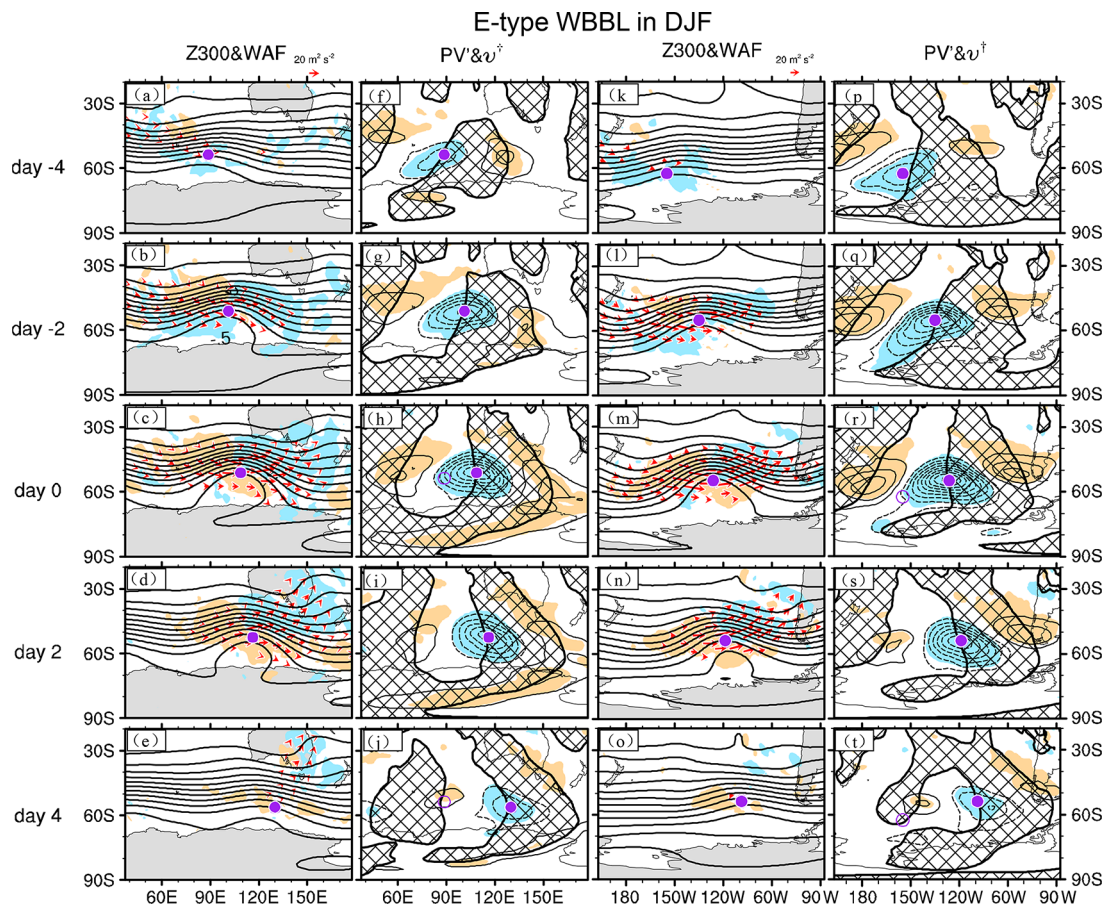


Fig. 10 As in Fig. 7 but for 30 E-type WBBL events at [50°S, 107.50°E] (first and second columns) and 24 E-type WBBL events at [53.75°S, 232.5°E] in austral summer

wave-activity flux emanating from the downstream flank of the amplifying pressure high (Fig. 11l-n).

4 Discussion

4.1 Transient eddy feedback forcing

The third column of Fig. 4 shows the transient eddy activity, which is represented as the high-frequency transient eddy kinetic energy (TEKE) at 300 hPa. The maximum TEKE appears over the South Atlantic and South Indian Oceans in summer and autumn. In contrast, winter exhibits the weakest TEKE over the midlatitude South Pacific (Fig. 4l), which could be attributed to the trapping effect of strong subtropical jet flow (Nakamura and Shimpo 2004). Generally, transient migratory eddies can facilitate low-frequency anomalies, including blocking highs, through feedback forcing (Illari and Marshall 1983; Shutts 1983; Colucci 1985; Holopainen and Fortelius 1987; Mullen 1987; Tsou and Smith 1990; Nakamura et al. 1997), with both barotropic (related to eddy vorticity flux convergence) and baroclinic

(linked to eddy heat flux convergence) forcings. The present study evaluated the two components through the geopotential tendency equation (Lau and Holopainen 1984) to discuss the roles played by transient eddies during the evolution of WB events.

Despite our calculations showing that composite transient eddy forcing contributes to the formation of WB events to some extent (not shown), these results generally lack statistical significance. However, there are instances where the impact of transient eddy forcing is notably significant. For instance, in the case of the 19 W-type WBBH events occurring at [73.75°S, 70°E] (first two columns of Fig. 8) and the 16 E-type WBBH events in austral winter at [72.5°S, 275°E] (last two columns of Fig. 9), transient eddy forcing accounts for approximately 10 to 30% of the amplification of the geopotential height around the primary PV center during the development stage. Overall, transient eddy forcing exhibits large case-to-case variability for WB events, making its influence marginal when examining the composite evolution of such events. Our findings offer indirect support to Wiedenmann et al. (2002), who speculated that the less frequent occurrence and shorter duration of

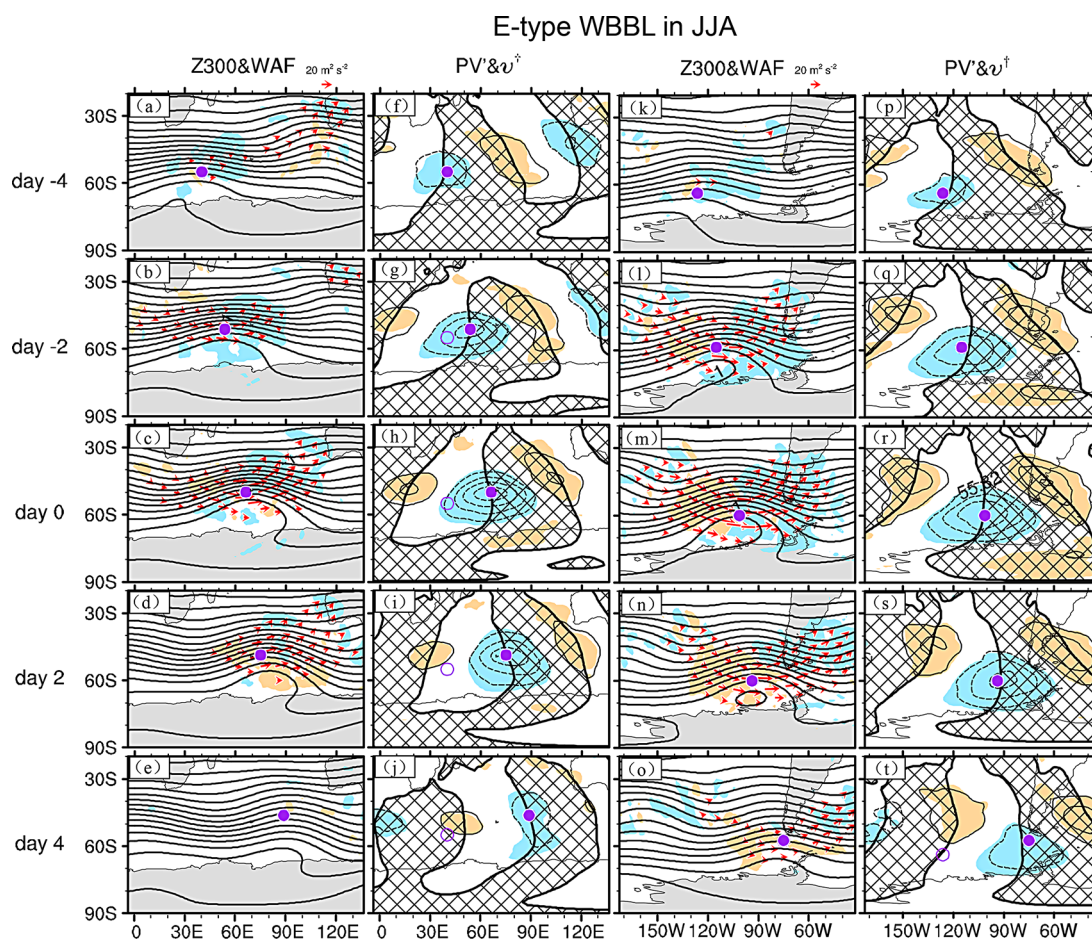


Fig. 11 As in Fig. 7 but for 28 E-type WBBL events at [51.25°S, 66.25°E] (first and second columns) and 27 E-type WBBL events at [61.25°S, 257.5°E] in austral winter

SH blocking compared to NH blocking might be due to the reduced interaction between transient eddies and planetary waves.

4.2 Long-term variation

Wiedenmann et al. (2002) reported a decreasing trend in SH blocking from 1970 to 2000. In contrast, Renwick (2005) demonstrated an increasing trend in the annual frequency of persistent positive anomalies over the SH from 1958 to 2001. In addition, Barriopedro et al. (2010) noted that there was a significant shift in the frequency of morphological SH WBs before and after 1979, with more frequent occurrences noted during the latter period when the abundance of satellite observation data increased. These results motivate us to explore whether long-term variation exists in our results, especially after 1979.

Figure 12 shows the numbers of high-amplitude WB events with blocking flow configurations poleward of 40°S, which are obtained by meridional summation every 11 years and within every zonal sector of 45° in longitude. Unlike

WBBH events, which predominantly cluster within the [150°E-120°W] sector, WBBL events occur more evenly in the zonal direction throughout the 66-year period. Overall, there was no abrupt change in frequency approximately 1979, except for the infrequent WBBL events observed over the [120°E-0°W] sector during the austral summer (Fig. 12f) and autumn (Fig. 12g) before 1979. This finding basically aligns with Renwick (2005), who reported that the climatological distribution of persistent positive anomalies remains largely unchanged upon removal of a linear trend from the daily height field.

Note that Fig. 12 also reveals some discernable long-term variations. For instance, after approximately 2000, WBBH events tend to occur less frequently over the [180°-150°W] sector in austral spring (Fig. 12a), while they become more frequent over the [0-60°E] and [150°E-140°W] sectors in austral autumn after 2000 (Fig. 12c) and over the [100-160°E] sector in austral winter after 1990 (Fig. 12d). Future studies on the physical mechanism of such long-term variations are needed.

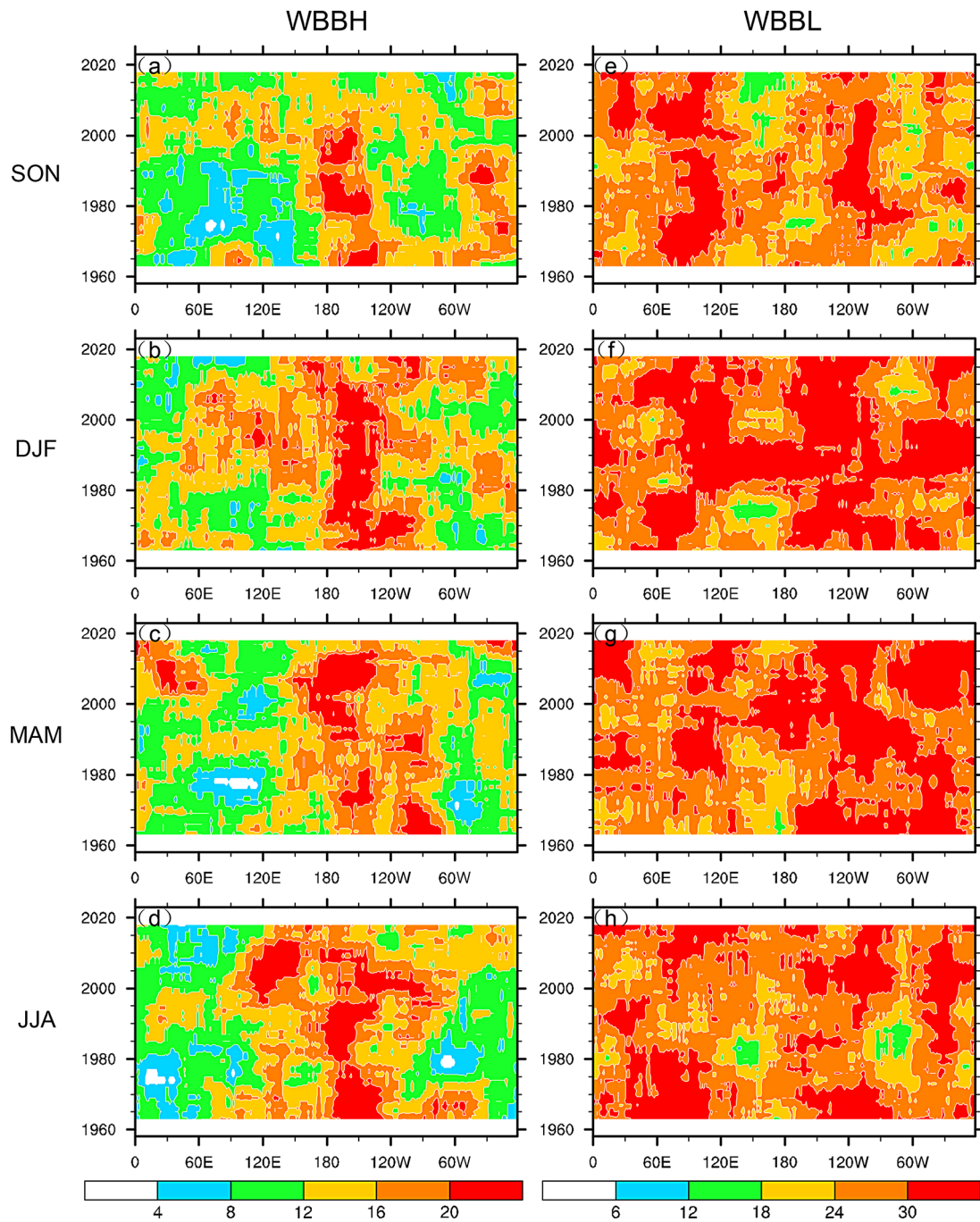


Fig. 12 Seasonal frequencies of (a-d) the WBBH events and (e-h) the WBBL events poleward of 40°S. The frequency is running summed by 11 years and 45° in longitude

The aforementioned main conclusions could also be verified by both the ERA5 and NCEP/NCAR reanalysis datasets, although ERA5 tends to identify the greatest number of events and NCEP/NCAR the least (Figs. S9 and 10).

5 Conclusions

The present work applies the detection method of high-amplitude wave breaking (WB) events with blocking flow configurations proposed by SN21 to the extratropical SH. SH WB events typically have a shorter characteristic timescale of approximately 5 days compared to approximately 9 days for NH events during boreal winter, reflecting the

more transient nature of SH circulation. The polarity of the primary height anomaly center classifies an event as a WB blocking high (WBBH) or blocking low (WBBL) event; the longitudinal movement of the primary PV anomaly center further categorizes events into eastwards (E), westwards (W), or stationary types.

Both WBBH events and WBBL events are prone to occur over the Antarctic continent, where climatological height eddies and westerlies are weak. However, their frequency distributions differ significantly over mid- and high-latitude oceans. WBBH events tend to be concentrated over the South Pacific, southeast Indian Ocean, and southwest Atlantic, whereas WBBL events are more uniformly distributed across the 45°S–60°S zonal belt throughout the year. These distribution differences are closely associated with the asymmetric influences of climatological flow on the formation of blocking flow configurations. In the South Pacific, strong positive height anomalies associated with high-pressure WB events often form a blocking high due to relatively weak climatological westerlies and overlying pressure ridges. In contrast, the formation of a blocking high is inhibited in the southern Indian Ocean and southern Atlantic due to the presence of strong polar jets and climatological pressure troughs. For high-amplitude low-pressure WB events, the climatological pressure ridge/trough and climatological westerlies become competitive in forming the blocking low configuration, resulting in a more uniform WBBL distribution. Note that most WB events are E-type events, while W-type events are more common over the Antarctic continent. Seasonality in preferred WB occurrence regions is not pronounced.

The Rossby wave breaking feature is identified through the reversal of the anomalous PV flux from negative to positive at the primary PV center, theoretically corresponding to a shift from convergence to divergence of the wave-activity flux. Composite analysis at several representative locations confirmed the consistency between the anomalous PV flux and wave-activity flux convergence/divergence, despite variations in the evolution of circulation anomalies and Rossby wave train propagation directions among different WB event types.

Although different meteorological fields and different detection methods are utilized, the frequency distribution characteristics of the selected WBBH events in the present study are generally consistent with previous studies on anticyclones (Sinclair 1996), blocking (Wiedenmann et al. 2002), morphological WB (Berrisford et al. 2007) or persistent circulation (Renwick 2005; Liu et al. 2017). For example, the South Pacific is one preferential region for their occurrence. This implies that these phenomena may represent different manifestations of a specific physical process and may be regulated by the background field. Note that

the present study provides a possible explanation for their formation, i.e., Rossby wave propagation. Clearly, our study extends the early studies by Renwick and Revell (1999) that emphasized the important role of Rossby wave propagation in blocking high formation over the southeast Pacific. In addition, in terms of the meridional direction, Ndarana and Waugh (2011) noted that there is no significant difference between different WBs in terms of equatorward or poleward PV intrusion. Accordingly, the classification of WB events into WBBH and WBBL types, as performed in the present study, appears more meaningful.

The wave-activity flux employed here is based on the assumption of a small-amplitude disturbance. For large-amplitude disturbances, Nakamura and Huang (2018) found that modulation by nonlinear zonal eddy flux becomes important. Therefore, using the finite-amplitude wave activity flux (Huang and Nakamura 2016) to evaluate the contribution of such nonlinear modulation for high-amplitude WB events should be a focus of future research. In addition, the diabatic process, which can break the conservation of PV, may be important in the formation of some blocking cases (e.g., Hirasawa et al. 2000; Tilly et al. 2008; Pfahl et al. 2015). Investigating the differences between WB events with and without strong diabatic effects is another important avenue for future studies.

Supplementary Information The online version contains supplementary material available at <https://doi.org/10.1007/s00382-024-07387-9>.

Author contributions All the authors contributed to the study conception and design. Material preparation, data collection and analysis were performed by Ning Shi and Tanimu Abubakar Sadiq. The first draft of the manuscript was written by Ning Shi and Tanimu Abubakar Sadiq. All the authors read and approved the final manuscript. Ning Shi is very grateful to Prof. Hisashi Nakamura for his encouragement and valuable suggestions on this study.

Funding This work is jointly supported by the National Natural Science Foundation of China (42088101), the Chinese Natural Science Foundation (41975063), the funding of the Jiangsu Innovation & Entrepreneurship Team and the Qing Lan Project.

Data availability The JRA-55 reanalysis data are available through the National Center for Atmospheric Research (USA): <https://rda.ucar.edu/datasets/ds628.0/>. The ERA5 reanalysis data are available at <https://cds.climate.copernicus.eu/cdsapp#!/dataset/reanalysis-era5-single-levels-monthly-meanstab=form>. The ERA5 reanalysis data are available at <https://psl.noaa.gov/data/gridded/data.ncep.reanalysis.html>. Figures were drawn using NCAR Command Language Version 6.6.2, which is available at <http://www.ncl.ucar.edu/>.

Declarations

Competing interests The authors have no relevant financial or non-financial interests to disclose.

References

- Altenhoff AM, Martius O, Croci-Maspoli M et al (2008) Linkage of atmospheric blocks and synoptic-scale rossby waves: a climatological analysis. *Tellus A* 60:1053–1063
- Barriopedro D, García-Herrera R, Trigo R (2010) Application of blocking diagnosis methods to general circulation models. Part I: a novel detection scheme. *Clim Dyn* 35:1373–1391
- Berrisford P, Hoskins BJ, Tyrlis E (2007) Blocking and Rossby Wave breaking on the Dynamical Tropopause in the Southern Hemisphere. *J Atmos Sci* 64:2881–2898
- Carpeneo CB, Ambrizzi T (2022) Atmospheric blockings in coupled Model Intercomparison Project Phase 5 models with different representations of Antarctic sea ice extent, vol 94. *Anais da Academia Brasileira de Ciências*, e20210432
- Colucci SJ (1985) Explosive cyclogenesis and large-scale circulation changes: implications for Atmospheric Blocking. *J Atmos Sci* 42:2701–2717
- Dunn-Sigouin E, Son SW, Lin H (2013) Evaluation of Northern Hemisphere blocking climatology in the global environment multiscale model. *Mon Wea Rev* 141:707–727
- Gabriel A, Peters DHW (2008) A diagnostic study of different types of Rossby Wave breaking events in the Northern Extratropics. *J Meteorol Soc Jpn* 86:613–631
- Hersbach H, Bell B, Berrisford P, Hirahara S, Horányi A, Muñoz-Sabater J, Nicolas J, Peubey C, Radu R, Schepers D, Simmons A, Soci C, Abdalla S, Abellan X, Balsamo G, Bechtold P, Biavati G, Bidlot J, Bonavita M, De Chiara G, Dahlgren P, Dee D, Diamantakis M, Dragani R, Flemming J, Forbes R, Fuentes M, Geer A, Haimberger L, Healy S, Hogan RJ, Hólm E, Janisková M, Keeley S, Laloyaux P, Lopez P, Lupu C, Radnoti G, de Rosnay P, Rozum I, Vamborg F, Villaume S, Thépaut J-N (2020) The ERA5 global reanalysis. *Q J R Meteorol Soc* 146:1999–2049
- Hirasawa N, Nakamura H, Yamanouchi T (2000) Abrupt changes in meteorological conditions observed at an inland Antarctic Station in association with wintertime blocking. *Geophys Res Lett* 27:1911–1914
- Holopainen E, Fortelius C (1987) High-frequency transient eddies and blocking. *J Atmos Sci* 44:1632–1645
- Holton JR (2004) An introduction to dynamic meteorology, 4th edn. Elsevier Academic Press, Cambridge, p 535
- Huang CSY, Nakamura N (2016) Local finite-amplitude wave activity as a diagnostic of anomalous weather events. *J Atmos Sci* 73:211–229
- Illari L, Marshall JC (1983) On the interpretation of Eddy Fluxes during a blocking episode. *J Atmos Sci* 40:2232–2242
- Kalnay E, Kanamitsu M, Kistler R, Collins W, Deaven D, Gandin L, Iredell M, Saha S, White G, Woollen J, Zhu Y, Chelliah M, Ebisuzaki W, Higgins W, Janowiak J, Mo KC, Ropelewski C, Wang J, Leetmaa A, Reynolds R, Jenne R, Joseph D (1996) The NCEP/NCAR 40-year reanalysis project. *Bull Am Meteorol Soc* 77:437–470
- Kidson JW (1999) Principal Modes of Southern Hemisphere low-frequency variability obtained from NCEP–NCAR reanalyses. *J Clim* 12:2806–2828
- Kobayashi S, Ota Y, Harada Y, Ebata A, Moriya M, Onoda H, Onogi K, Kamahori H, Kobayashi C, Endo H, Miyaoka K, Takahashi K (2015) The JRA-55 reanalysis: general specifications and basic characteristics. *J Meteorological Soc Japan Ser II* 93:5–48
- Lau N-C, Holopainen EO (1984) Transient eddy forcing of the time-mean flow as identified by geopotential tendencies. *J Atmos Sci* 41:313–328
- Liu P, Zhu Y, Zhang Q, Gottschalck J et al (2017) Climatology of tracked persistent maxima of 500-hPa geopotential height. *Clim Dyn* 51:701–717
- Martius O, Schwierz C, Davies HC (2007) Breaking Waves at the Tropopause in the wintertime Northern Hemisphere: climatological analyses of the orientation and the theoretical LC1/2 classification. *J Atmos Sci* 64(7):2576–2592
- Masato G, Hoskins BJ, Woollings TJ (2012) Wave-breaking characteristics of midlatitude blocking. *Q J R Meteorol Soc* 138:1285–1296
- Masato G, Hoskins BJ, Woollings T (2013) Wave-breaking characteristics of northern hemisphere winter blocking: a two-dimensional approach. *J Clim* 26:4535–4549
- Mullen SL (1987) Transient eddy forcing of blocking flows. *J Atmos Sci* 44:3–22
- Nakamura H (1994) Rotational evolution of potential vorticity associated with a strong blocking flow configuration over Europe. *Geophys Res Lett* 21:2003–2006
- Nakamura H, Fukamachi T (2004) Evolution and dynamics of summertime blocking over the Far East and the associated surface Okhotsk high. *Q J R Meteorol Soc* 130:1213–1233
- Nakamura H, Shimpo A (2004) Seasonal variations in the Southern Hemisphere Storm tracks and Jet streams as revealed in a Reanalysis dataset. *J Clim* 17:1828–1844
- Nakamura H, Nakamura M, Anderson JL (1997) The role of high-and low-frequency dynamics in blocking formation. *Mon Weather Rev* 125:2074–2093
- Nakamura N, Huang CS, Y (2018) Atmospheric blocking as a traffic jam in the jet stream. *Science* 361:42–47
- Ndarana T, Waugh DW (2011) A climatology of Rossby Wave breaking on the Southern Hemisphere Tropopause. *J Atmos Sci* 68:798–811
- Nishii K, Nakamura H (2004) Lower-stratospheric Rossby wave trains in the southern hemisphere: a case-study for late winter of 1997. *Q J R Meteorol Soc* 130:325–345
- Nishii K, Nakamura H, Orsolini YJ (2011) Geographical dependence observed in blocking high influence on the stratospheric variability through enhancement and suppression of upward planetary-wave propagation. *J Clim* 24:6408–6423
- Pelly JL, Hoskins BJ (2003) A New Perspective on blocking. *J Atmos Sci* 60:743–755
- Peters D, Waugh DW (1996) Influence of Barotropic Shear on the Poleward Advection of Upper-Tropospheric Air. *J Atmos Sci* 53:3013–3031
- Peters D, Waugh DW (2003) Rossby Wave breaking in the Southern Hemisphere Wintertime Upper Troposphere. *Mon Weather Rev* 131:2623–2634
- Pfahl S, Schwierz C, Croci-Maspoli M et al (2015) Importance of latent heat release in ascending air streams for atmospheric blocking. *Nat Geosci* 8:610–614
- Renwick JA (2005) Persistent positive anomalies in the southern hemisphere circulation. *Mon Weather Rev* 133:977–988
- Renwick JA, Revell MJ (1999) Blocking over the South Pacific and Rossby Wave Propagation. *Mon Weather Rev* 127:2233–2247
- Rivière G, Lainé A, Lapeyre G, Salas-Méla D, and Kageyama M (2010) Links between Rossby Wave Breaking and the North Atlantic Oscillation–Arctic Oscillation in present-day and last glacial maximum climate simulations. *J Clim* 23:2987–3008
- Schwierz C, Croci-Maspoli M, Davies HC (2004) Perspicacious indicators of atmospheric blocking. *Geophys Res Lett* 31:L06125
- Seaman R, Hart T (2003) The history of PAOBs in the Australian Bureau of Meteorology. *Aust Meteorol Mag* 52(4):241–250
- Shi N, Nakamura H (2021) A new detection scheme of wave-breaking events with blocking flow configurations. *J Clim* 34:1467–1483
- Shutts GJ (1983) The propagation of eddies in diffluent jetstreams: Eddy Vorticity forcing of ‘blocking’ flow fields. *Q J R Meteorol Soc* 109:737–761
- Sinclair MR (1996) A climatology of anticyclones and blocking for the Southern Hemisphere. *Mon Weather Rev* 124:245–264

- Small D, Atallah E, Gyakum JR (2014) An objectively determined blocking index and its northern hemisphere climatology. *J Clim* 27:2948–2970
- Strong C, Magnusdottir G (2008) Tropospheric Rossby Wave Breaking and the NAO/NAM. *J Atmos Sci* 65(9):2861–2876
- Takaya K, Nakamura H (2001) A formulation of a phase-independent wave-activity flux for stationary and migratory quasigeostrophic eddies on a zonally varying basic flow. *J Atmos Sci* 58:608–627
- Takaya K, Nakamura H (2005) Geographical dependence of Upper-Level blocking formation Associated with Intraseasonal amplification of the siberian high. *J Atmos Sci* 62:4441–4449
- Thompson DW, Solomon S (2002) Interpretation of recent Southern Hemisphere climate change. *Science* 296:895–899
- Thornicroft CD, Hoskins BJ, McIntyre ME (1993) Two paradigms of baroclinic-wave life-cycle behaviour. *Q J R Meteorol Soc* 119:17–55
- Tilly DE, Lupo AR, Melick CJ, Market PS (2008) Calculated height tendencies in two Southern Hemisphere Blocking and Cyclone events: the contribution of Diabatic Heating to Block Intensification. *Mon Weather Rev* 136:3568–3578
- Trenberth KE, Mo KC (1985) Blocking in the Southern Hemisphere. *Mon Weather Rev* 113:3–21
- Tsou C-H, Smith PJ (1990) The role of synoptic/planetary-scale interactions during the development of a blocking anticyclone. *Tellus A: Dynamic Meteorol Oceanogr* 42:174–193
- Tyrlis E, Hoskins BJ (2008) The morphology of Northern Hemisphere Blocking. *J Atmos Sci* 65:1653–1665
- Weijenborg C, Vries H, Haarsma RJ (2012) On the direction of Rossby wave breaking in blocking. *Clim Dyn* 39:2823–2831
- Wiedenmann JM, Lupo AR, Mokhov II et al (2002) The climatology of blocking anticyclones for the Northern and Southern hemispheres: Block Intensity as a diagnostic. *J Clim* 15:3459–3473
- Wilks DS (2016) The stippling shows statistically significant Grid points: how Research results are routinely overstated and over-interpreted, and what to do about it. *Bull Am Meteorol Soc* 97:2263–2273
- Williams LN, Lee S, Son SW (2007) Dynamics of the southern hemisphere spiral jet. *J Atmos Sci* 64:548–563
- Wolf G, Wirth V (2017) Diagnosing the horizontal propagation of Rossby Wave packets along the Midlatitude Waveguide. *Mon Weather Rev* 145:3247–3264
- Wolf G, Brayshaw DJ, Klingaman NP, Czaja A (2018) Quasi-stationary waves and their impact on European weather and extreme events. *Q J R Meteorol Soc* 144:2431–2448

Publisher's Note Springer Nature remains neutral with regard to jurisdictional claims in published maps and institutional affiliations.

Springer Nature or its licensor (e.g. a society or other partner) holds exclusive rights to this article under a publishing agreement with the author(s) or other rightsholder(s); author self-archiving of the accepted manuscript version of this article is solely governed by the terms of such publishing agreement and applicable law.